Quasi-Static Analysis of hip cement spacers

Abdelhafid Mallek[1], Abdelkader Miloudi[2] , Mokhtar Khaldi[3], Mohammed-Mokhtar Bouziane [1,3,*], Belabbes Bachir Bouiadjra[1], Habiba Bougherara[4], Richie H.S Gill[5]

[1] LMPM, Department of Mechanical Engineering, University of Sidi Bel Abbes, BP 89, Cité Ben M'hidi, Sidi Bel Abbes 22000, Algeria
[2] LMSR, Department of Mechanical Engineering, University of Sidi Bel Abbes, BP 89, Cité Ben M'hidi, Sidi Bel Abbes 22000, Algeria

[3] Department of Mechanical Engineering, Faculty of Technology, University of Mascara, BP 305 Route de Mamounia, Mascara 29000, Algeria
[4] Department of Mechanical and Industrial Engineering, Ryerson University, Toronto, Ontario, Canada
[5] Centre for Orthopedic Biomechanics, Department of Mechanical Engineering, University of Bath, Bath, United Kingdom

* Corresponding author: e-mail: m.bouziane@univ-mascara.dz

Abstract

The use of temporary hip prosthesis made of orthopedic cement (spacer) in conjunction with antibiotics became a widespread method used for treating prosthetic infections despite the fact that this method makes bone cement (PMMA)more fragile. The necessity to incorporate a reinforcement is therefore crucial to strengthen the bone cement. In this study, a validated Finite Element Modelling (FEM) was used to analyze the behavior of spacers. This FEM model uses a non-linear dynamic explicit integration to simulate the mechanical behavior of the spacer under quasi-static loading. In addition to this FEM, Extended Finite Element Method (XFEM)was also used to investigate the fracture behavior of the spacers reinforced with titanium, ceramic, and stainless-steel spacer stems. The effect of the material on the performance of the reinforced spacers was also analyzed. The results showed that numerical modelling based on explicit finite element using ABAQUS/Explicit is an effective method to predict the different spacers' mechanical behavior. The simulated crack initiation and propagation were in a good agreement with experimental observations. The FEM models developed in this study can help mechanical designers and engineers to improve the prostheses' quality and durability.

Keywords: Orthopedic Hip Spacer, Quasi-static, Brittle cracking, XFEM, Reinforcement

1 Introduction

Joint replacement infections can occur during or after total hip replacement (THR) surgeries. One commonly used technique to treat such infections is to perform THR in two stages using a temporary prosthesis called a “Spacer”. Spacers are generally made of bone cement and contain one or more antibiotic to target specific types of infections [1-5]. However, these spacers are relatively fragile which pose an increased risk of sudden fracture [6-7]. Numerous medical reports on patients who underwent a two-stage implantation indicated failure of the spacer resulting from a very moderate physical activity [8-9]. It is believed that the addition of antibiotics to the cement disrupted the polymerization phase of the cement via the modification of the powder/monomer ratio [7], which in turn increased the amount of non-activated residuals and un-cured monomers. In addition, the non-homogeneity characteristics of the cement made it less resistant. Due to the lack of studies regarding the adaptability of various spacers’ models available on markets [10, 11], the Orthopedic Department of the Saarland University Hospital has designed its own spacer to adjust the antibiotic concentration intra-operatively during surgery (Fig.1).This spacer has been the subject of two studies to evaluate the cyclic and monotonic loads the spacer can withstand without failure and established the loading limits for different types of reinforcement. [12-13]. Non-linear static analysis was used in many studies for different modelling under quasi-static loading. Due to computers capacity limitation, the first study which was developed using two-dimensional (2D) FE models [14-16] showed that 2D models are not appropriate to accurately predict mechanical behavior of the spacer. The advanced computing capabilities, on the other hand, allowed many researchers to develop three dimensional-implicit method (3D) models to analyze different geometries under different loading conditions [17-19]. However, the simulation process encountered issues related to the convergenceand the complexity of the geometry. To overcome convergence difficulties, several researchers performed dynamic analysis which showed a good correlation between numerical and experimental results [20,21]. The explicit integration method has also been used to analyze the mechanical behavior of the different designs under quasi-static loading [22]. For instance, the Extended Finite Element Method (XFEM)has proven to be highly effective in predicting the crack initiation and subsequent propagation [24]. Investigating crack propagation is vital to avoid sudden fracture and prevent from prosthesis loosening [25]. Numerous researchers have investigated experimentally the mechanical behavior of spacers showing the benefits of adding reinforcements [12,26,27,28]. While there are very few numerical studies on hip

spacers [13,29], none of them have been validated, or can be used to predict the propagation of the crack in the spacer.

The aim of this study is twofold, the first is to create and validate a realistic numerical model to simulate the mechanical behavior of the spacer under quasi-static load, and secondly, to optimize the geometry of a hip spacer and reduce its cost. Numerical results were compared with the experimental tests results of hip spacer to validate the FE model. In addition, the mainfactors influencing the model were also discussed.

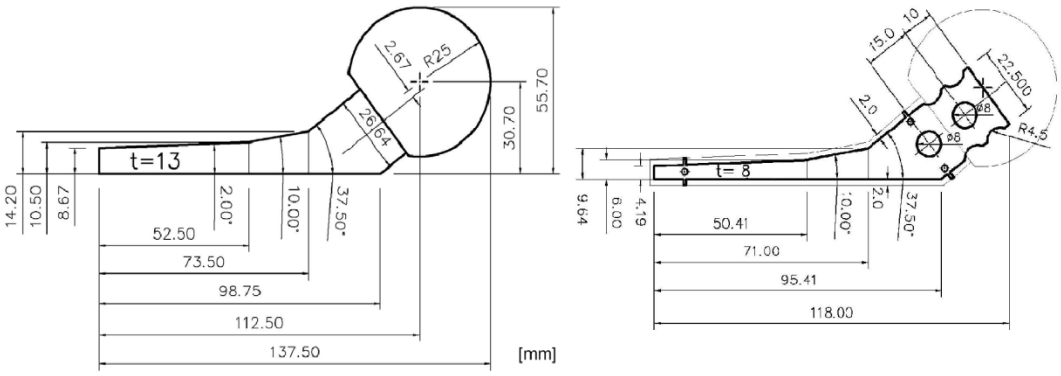

Fig.1 Dimensions of the spacer and the reinforcement [13].

2 Finite element analysis

3D numerical models illustrating the T. Thielen experimental specimens were developed for each type of spacer using ABAQUS software [12]. The head of the spacer has 50mm diameter, and the stem length is 100mm with a surface area of 13,300mm^2. The stem is inserted 60mm in polyurethane (PU) cylinder and was inclined by 10° according to the frontal plane and by 9° according to the sagittal plane (Fig.2).

In the present study, a frictionless contact between the applicator and the femoral head was achieved by replacing the Polyoxymethylene (POM) cylinder used in the experimental tests [12] by a half-sphere. Such modification to ensure a unique point-to-point contact between applicator and spacer head. The displacement is imposed on a reference point placed on the upper face of the half sphere, which is connected to a part of this surface using Multi-point constraints (MPC). A particular subdivision process was adopted to build structured meshes for the spacer and its reinforcement in order to minimize the computation time.

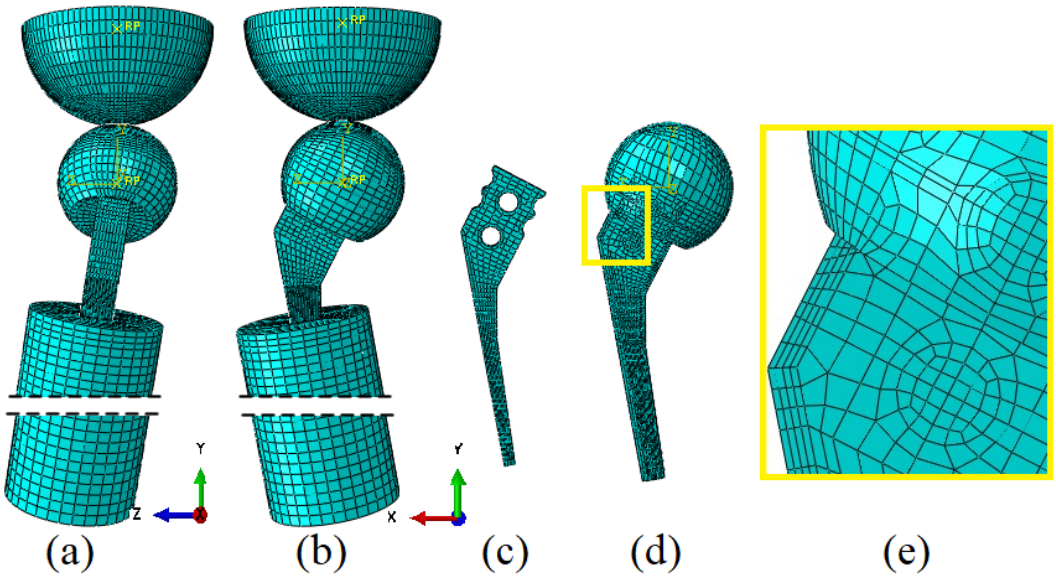

Fig. 2. Finite element meshes of hip prosthesis components: (a)posterior view of hip spacer, (b)lateral view of hip spacer, (c)endoskeleton, (d)implant and (e) spacer's high bending zone.

2.1 Analysis Strategy

The implicit and the explicit approaches for solving quasi-static problems were achieved via ABAQUS software. The implicit method commonly called “ABAQUS/Standard” used the Newton-Raphson method to solve nonlinear problems by inversing stiffness matrix. Hence, this process is applied for each loop. On the other hand, ABAQUS/Explicit uses an integration scheme based on central difference method which minimizes the computational time when compared to the implicit one. Thus, the explicit algorithm ensures sufficient robustness leading to a more effective and complete calculation than the implicit method, particularly for complex contact models [22]. Other advantages of ABAQUS/Explicit include the use of less RAM and disk space compared to ABAQUS/Implicit, and efficacy in solving quasi-static problems only by minimizing the inertia effects [22, 23].

2.2 Element Type and Contacts modeling

The 3D geometry of the construct (Fig. 2) was meshed using hexahedral elements with eight nodes (C3D8R). These elements allow for geometrical and material nonlinearity and provide a solution with a good accuracy and with less computation time. Nonetheless, the use of the reduced integration scheme has a drawback which can result mesh instability, commonly referred to as “hourglassing” [23]. To avoid this issue, at least four elements were used in the bending regions (Fig.2(e)), and the contact stress was distributed between several nodes using surface to surface contact algorithm [23]. The contact modeling is one of the most important

steps for a more accurate analysis. Therefore, the choice between different interaction properties significantly influences the accuracy of results. Tie contact with surface-to-surface formulation was used to model the contact between the reinforcement and the spacer, as well as between the spacer and the cylinder. This enables to capture the stresses and deformations stably and quickly [30,31]. To define the interaction between the applicator and the head of the prosthesis, a tangential frictionless contact and normal hard contact allowing the separation between the different used surfaces.

2.3 Materials Properties

The elastic properties of the different materials selected for this simulation are the same used by T. Thielen [12, 13], and are presented in Table 1. The plastic properties of Titanium grade II (fig. 3) were determined from the nominal stress-strain curve of Ti40 [32]. However, the true Stresses-strains (σ_{True}–ε_{True}) are calculated from the nominal values according to the following equations:

$$\sigma_{True}=\sigma_{Eng}\ (1+\varepsilon_{Eng})\ (1)$$

$$\varepsilon_{True}=Ln\ (1+\varepsilon_{Eng})\ (2)$$

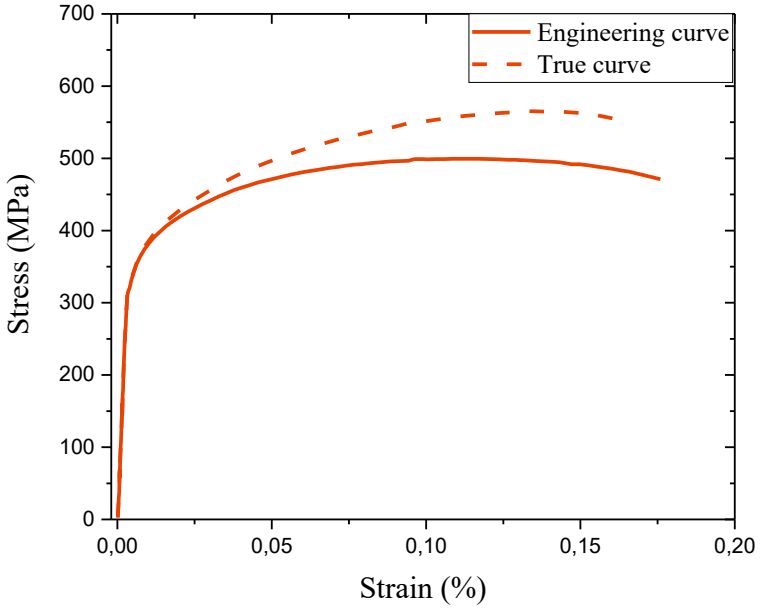

Fig. 3 Stress-strain curves of Titanium grade II [32].

2.4 Loading and Boundary conditions

The boundary condition was applied by fixing the distal end of the cylinder. In addition, a displacement is imposed on a reference point placed on the upper face of the hemisphere, which is connected to a part of this face by a multi-point constraint (MPC). The mobility of

this point is limited to a translation and a rotation towards the Y axis. Consequently, the loading was applied as an imposed displacement. In the case of explicit analysis, the displacement loading amplitude must be applied smoothly and progressively; because the sudden and irregular movements can generate stress waves which induce imprecise (noisy) or irregular results [23]. The loading rate is defined as the ratio of the total displacement over the step time. This rate should be relatively low to eliminate the dynamic effects but not very small to avoid the increase of calculation time. Also, the use of an adequate mass scaling factor can reduce the calculation time with the conservation of a low loading rate.

Table 1 Material properties used for the analysis [12]

Materials	Young modulus [MPa]	Poisson ratio	Density [Kg/m^3]
PMMA	2500	0.35	1188
Polyurethane (PU)	4100	0.35	1010
Polyoxymethylene (POM)	3100	0.35	1010
Titanium grade II	110000	0.34	4500

2.5 Comparison of the numerical results with experimental tests

Before verifying the validity of the numerical results obtained with the explicit method, the results should satisfy the quasi-static behavior (Fig. 4). As such, to validate the results, we should satisfy two conditions. First, the ratio value of kinetic energy and internal energy of the whole assembly model should not exceed 5% during the whole analysis process. And second, absence of local deformations.

The satisfaction of the two above conditions are sufficient to ensure that the effect of inertia is negligible (i.e., ensuring quasi-static behavior). It is also necessary to check the absence of kinetic energy oscillation. For this case, the oscillations will be eliminated by applying progressive and smoother load amplitude and/or by the addition of a damping factor to the materials properties. Hence, the applied factor must be as small as possible to avoid a large increase of viscous energy dissipation [23].

Practically, for the purpose of reducing the calculation time, it is necessary to start the simulations with a fast loading rate and apply several test series with different mass scaling and checking each step that the results satisfy the above-mentioned conditions.

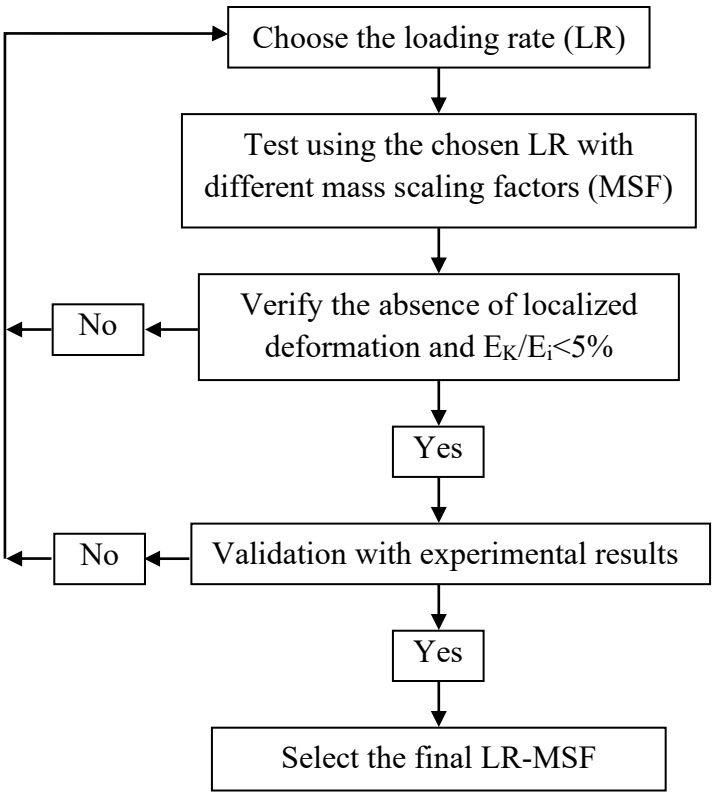

Fig. 4 Validation algorithm Flowchart of the numerical model [22].

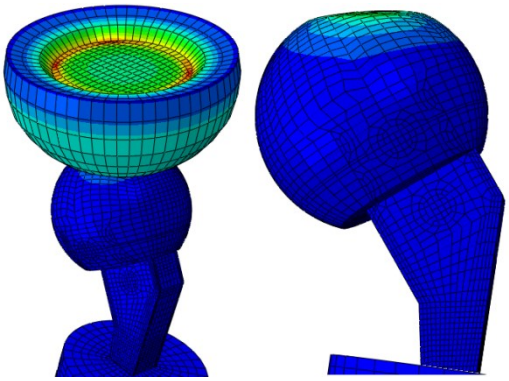

(a) Loading rate = 10mm/s

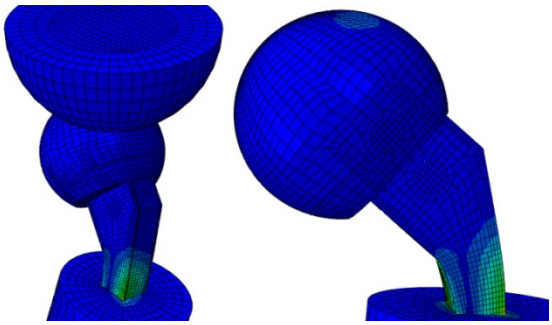

(b) Loading rate = 0.5mm/s

Fig.5 Deformation of the spacer at different loading rates

In this study, four models of spacer were validated with four spacer types tested by Thielen et al (non-reinforced spacer, full-stem reinforced spacers with titanium endoskeleton of 6mm, 8mm and 10mm of thickness) concerning load-displacement relationships [12] and deformed shapes. The test was conducted as a sample to demonstrate this strategy. In this case, the test was performed with full-stem reinforced spacer with titanium endoskeleton of 10mm. The first test is carried out by setting the mass scaling factor to 10^7 and varying the loading rate regressively from a relatively high value of 10 mm/s to a low value of 0.5 mm/s. Fig.5(a) shows highly localized deformations caused by the large inertia forces occurring during high speed loading. Therefore, the short time test avoiding stresses wave to stretch along the entire prosthesis; consequently, only the top of the head has been deformed. The fig.5(b)presents that, the use of a lower speed loading generates a high level of stresses around the stem of the spacer. However, even with a loading rateof 0.5mm/s (Fig.6(a)), the ratio between the kinetic energy and the internal energy is greater than 5% due to the introduction of a high mass scaling factor. Fig.6(b) shows that the use of a mass scaling factor of 10^6 reduces the effect of inertia. It is concluded that, all tests carried out with a speed of 0.5 mm/s and a mass scaling factor less than or equal to 10^6 can be considered as quasi-static.

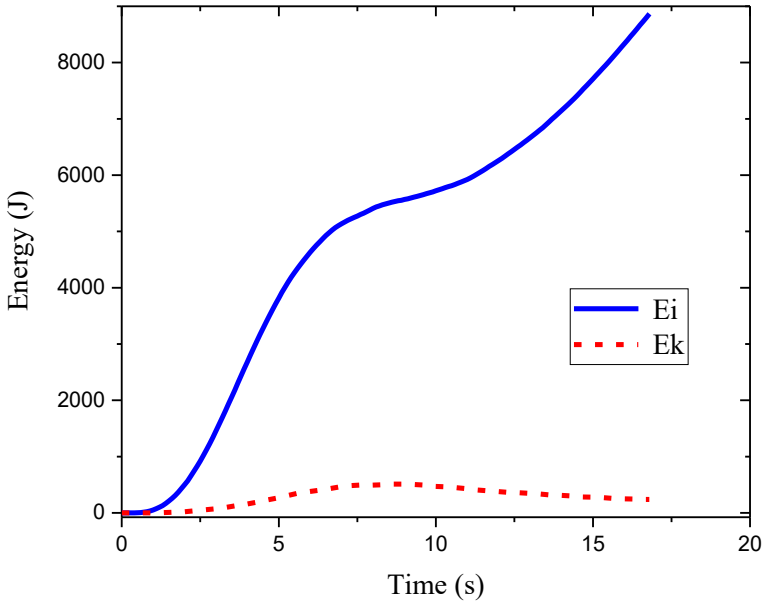

Fig.6(a): Energy-time relationship with LR = 0.5mm/s and MSF = 10^7

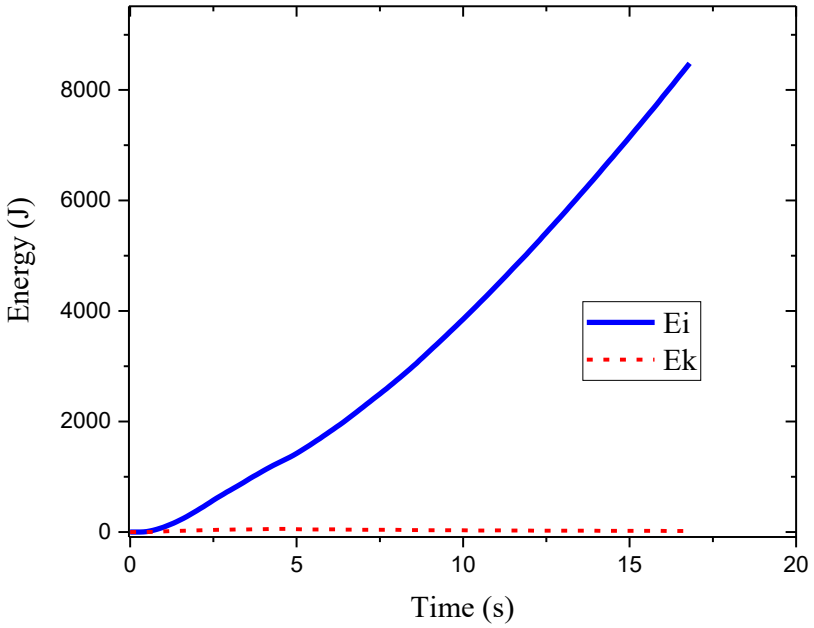

Fig.6(b): Energy-time relationship with LR = 0.5mm/sandMSF = 10^6

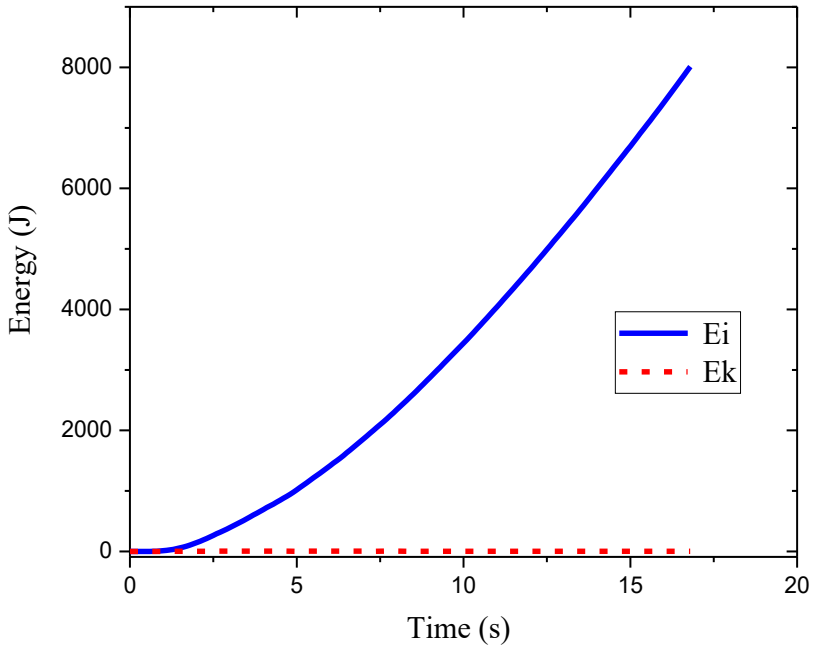

Fig.6(c): Energy-time relationship with LR = 0.5mm/s andMSF = 10^5

The combination of a speed of 0.5 mm/s and a mass scaling of 10^5 permits to the validation of the numerical and experimental results for the spacer with 10mm reinforcement. Numerical parameters for the other three spacers type are also listed in Table 2.

Table 2 LR-MSF values allowing the validation for four models of spacer

Spacer type	Non-reinforced spacer	Reinforced spacers with 6mm thickness endoskeleton	Reinforced spacers with 8mm thickness endoskeleton	Reinforced spacers with 10mm thickness endoskeleton
Loading rate(mm/s)	0.07	0.3	0.4	0.5
Mass scaling factor	10^5	10^5	10^5	10^5

Figures 7 shows a comparison of the force-displacement curves obtained numerically with both explicit and implicit methods versus the curves obtained from the experimental results [12]. These results demonstrate that the numerical model using the explicit method is able to predict the mechanical behavior of both reinforced and non-reinforced spacer under quasi-static loading. The values of the forces obtained using the explicit method are greater than the implicit method, which can be justified by the fact that ABAQUS/Explicit regularizes the material data [23].

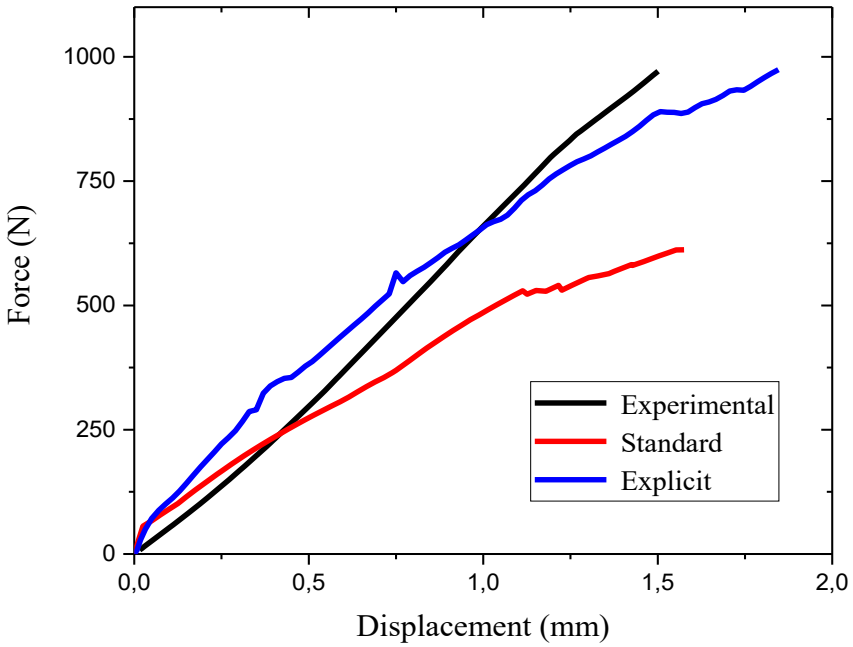

(a) Non-reinforced spacer

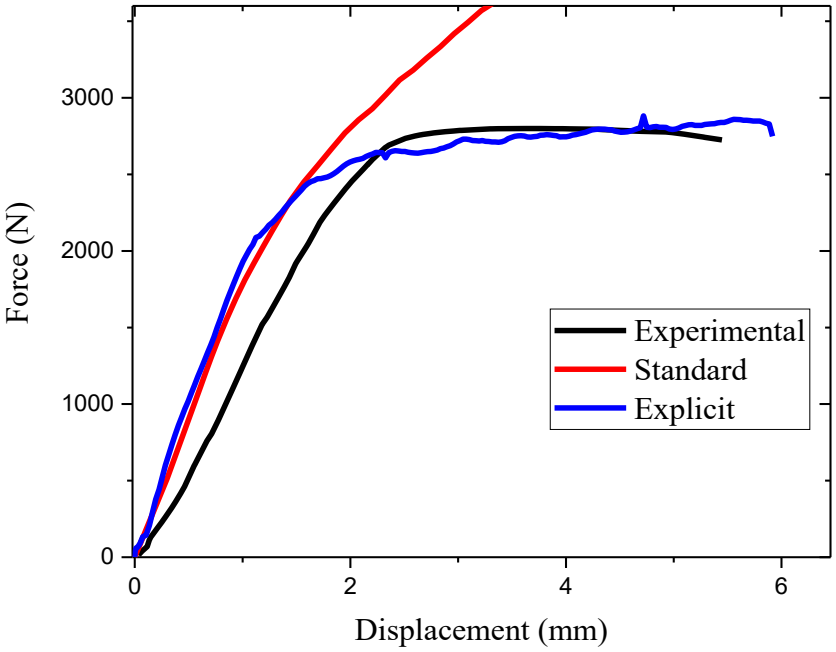

(b) Reinforced spacers with 6mm thickness endoskeleton

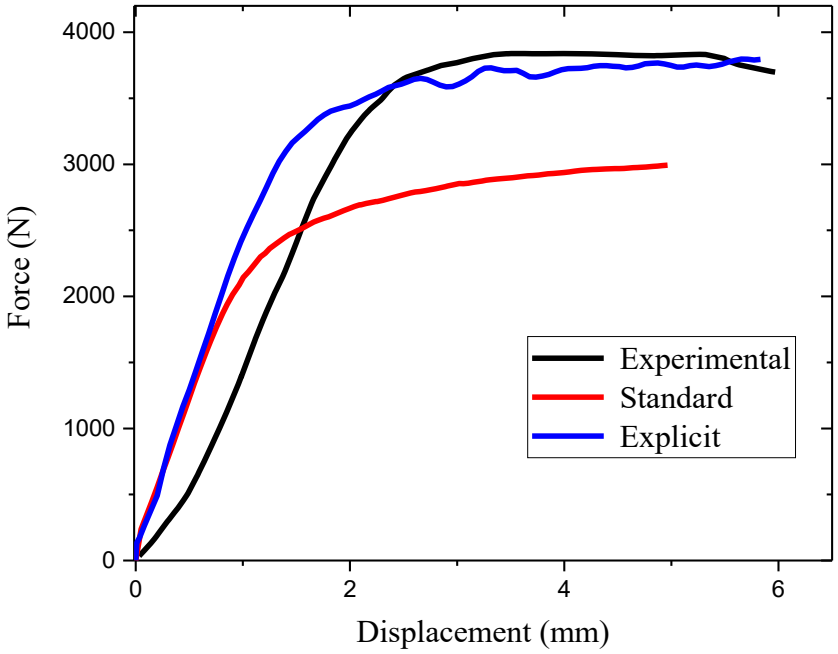

(c) Reinforced spacers with 8mm thickness endoskeleton

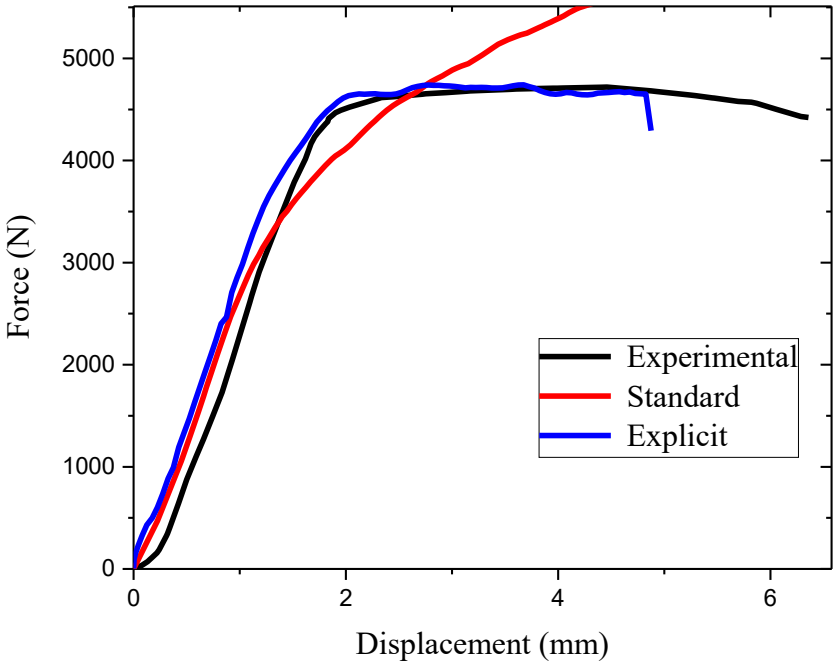

(d) Reinforced spacers with 10mm thickness endoskeleton

Fig.7 Verification of the load displacement curve of the numerical models and the experimental results of the different types of spacers [12].

3. Fracture behavior of spacers

One of the main drawbacks of fragile materials, is their low tensile strength which can lead to crack formation, and reduction in the stiffness of the material. Therefore, the formulated constitutive laws for a tough material are not valid in the presence of a crack. To model cracks in materials with high toughness one can applied cohesive forces to the lips of a crack initiated by the XFEM method (discrete crack model) or use diffuse method (smeared crack). This second approach (continuous crack model) was developed initially for the cement, which allows for a better description of the damage behavior due to fragile materials cracking. Subsequently, stresses and strains are evaluated at an integration points; and the material properties degradation affects the region surrounding these points and diffuses the crack effects in this region. Therefore, the continuous cracking process removes the mesh discontinuity.

3.1 The brittle failure criterion

The non-cracked PMMA behavior is considered linear, isotropic, and elastic under tensile loads. A simple Rankine criterion is only used to detect the crack initiation in mode I.

Practically, the principal stresses and its directions are calculated at an integration point and consequently in the case of positive stresses, and when exceeding a limit value, a crack appears perpendicular to the direction of these stresses at the considered point. It is assumed that the post-crack behavior includes both mode I and mode II. The mode I is specified by means of direct stress-strain relationship of a post-cracking, or by specifying the mode I fracture energy assuming a linear stress-strain relationship [33]. The shear behavior by mode II is based on the observation of shear modulus reduction when the crack opens. ABAQUS/Explicit proposes a shear retention model in which the post-crack shear stiffness is defined according to the strain across the crack opening. When one, two, or three components of the direct local stress of the crack (displacement) reach the defined value as rupture stress (displacement), all stress components are set to zero as materials point. If all of the material points in an element fail, the element is removed from the mesh [23].

3.2 XFEM criterion

The XFEM is an alternative modeling approach to the classical finite elements method (FEM) for solving cracked structures. The use of this method allows the modeling of the transition from damage to failure by improving an existing mesh with shape functions capable of representing discontinuities in zones and gradients in addition to singularities. The XFEM method was implemented by modeling the crack with cohesive behavior [34-37]. Such approach gives the possibility for modeling the crack initiation and propagation through any arbitrary path, thus exploiting the advantages of the XFEM methods and the cohesive zone. In such combination, the asymptotic singularity near the extremity is replaced by a cohesive zone and only the displacement progression through a completely cracked element is taken into account. Consequently, the crack should propagate throw an entire element at one time to avoid modeling the stresses singularity.

The cohesive models are based on zone process assumption described as a fictive interface along which the displacement field can admit discontinuities, during continuing forces transmission. This model has been improved [33] by introducing the fracture energy concepts G_c (surface energy necessary to separate the two crack lips at an interface point) and critical stress (maximum stress value in which the crack is supposed to propagate). The two material parameters characterize an interface law called a traction-separation law (Fig. 8), relating the stress to the displacement vector. The sum of the total energy dissipated during the creation of

a discontinuity (when T_{ult} is reached) and until a complete rupture is the cohesive crack energy G_c.

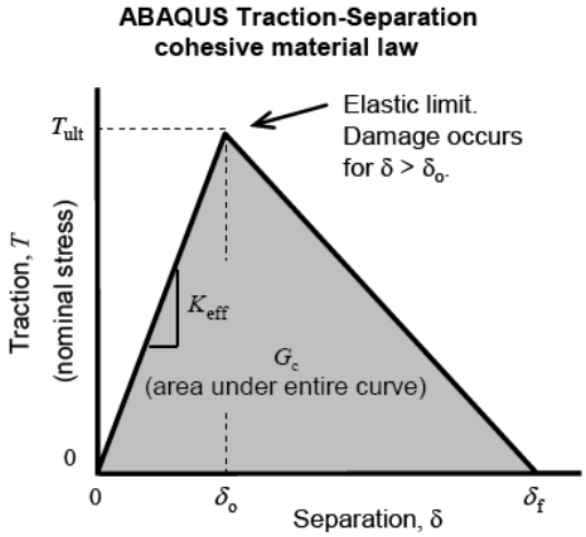

Fig. 8 Traction separation law used in the model

3.3. Numerical modeling

ABAQUS/Explicit allows to model the crack propagation process by involving the brittle cracking material model; the material parameters used were adapted according to the study of Khan et al. which validated PMMA indentation model. The initiation of crack occurs when the maximum principal stress exceeds the tensile failure limit of the orthopedic cement, and the modeling of the crack behavior is described by the stress/strain relationship after cracking, or by applying the failure energy criterion [38].Since, the post-crack behavior has been described in terms of stress/failure energy, the brittle failure criterion allows the removal of damaged elements from the mesh. Thus, the failure displacement must be given as the failure criterion [23]. The modeling of the discrete crack by the XFEM method is carried by the ABAQUS/standard. The required parameters for the crack initiation (ultimate tensile strength) and crack propagation (fracture energy) are the same for the brittle crack modeling (Table3) [38]. In the experimental study, the crack occurred at the spacer stem level, thus, this area has been meshed by refined elements especially in the model of brittle fracture where the crack visualization is done through defective elements suppression.

Table 3 Failure properties of the PMMA [38,39]

Material parameters	**Values**	
Tensile strength (MPa)	35	
Fracture energy (J/m^2)	400	
Direct cracking failure	0.02	
Brittle shear	**Shear retention factor**	**Crack opening**
	1	0
	0.5	0.001
	0.25	0.002
	0.125	0.003

3.4 Fracture Results

The comparison between experimental tests[12] ,the brittle cracking and XFEM models show that, the crack was initiated from the left posterior side just above the insertion into the PU cylinder, and extends to the back and left sides (Fig.10).In the brittle cracking model, the crack propagation is more important and extends to the front edges. In addition, the two numerical models of non-reinforced spacer (Fig.10 (a)) do not reach the total rupture of the spacer. For the other cases (i.e, spacers with reinforcement of 6, 8, and 10 mm), the deformation behavior of numerical models is identical to the deformation of experiment models (Fig. 10 (b-d)). Figures11&12 illustrate the distribution of the maximum principal stresses (crack initiation criterion in both models) during the crack propagation stages.

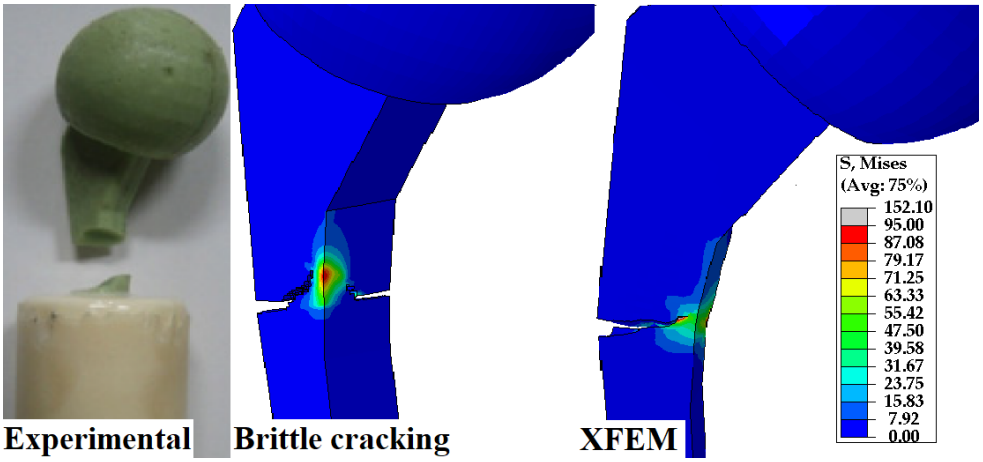

(a)Non-reinforcement Spacer

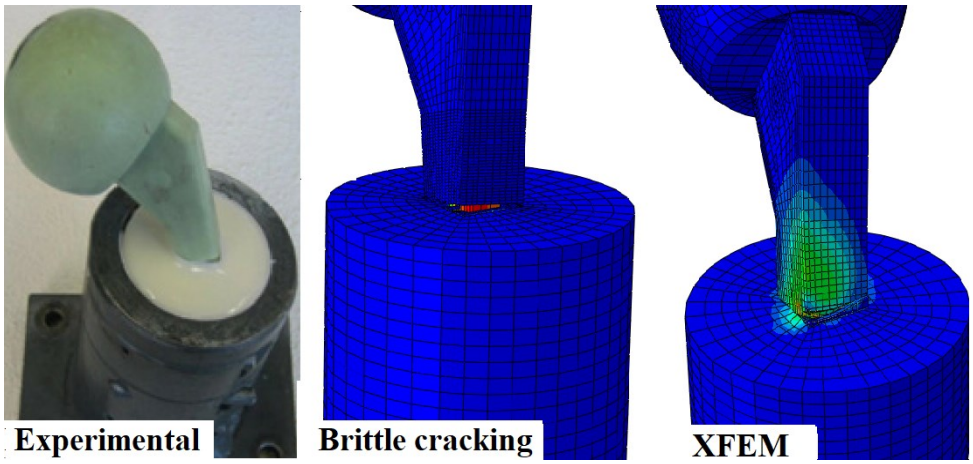

(b)Full-stem reinforced spacers with 6mm thickness endoskeleton

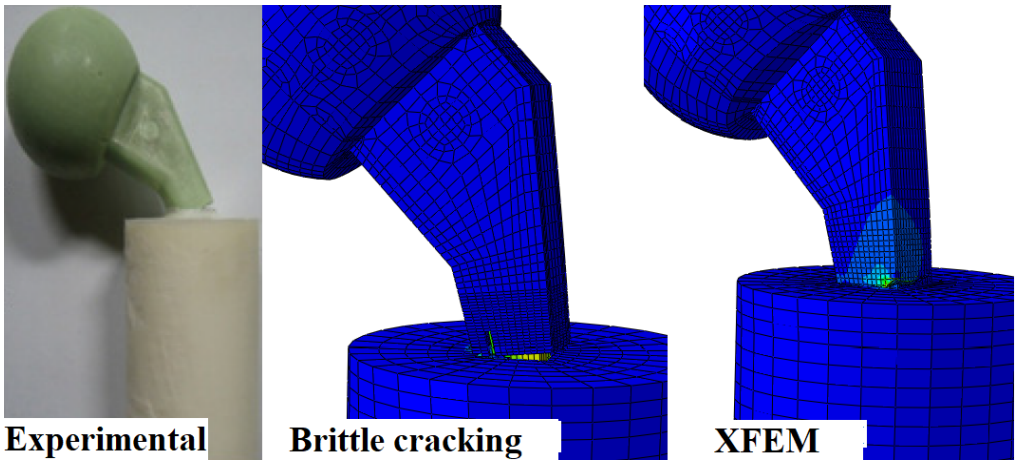

(c) Full-stem reinforced spacers with 8mm thickness endoskeleton

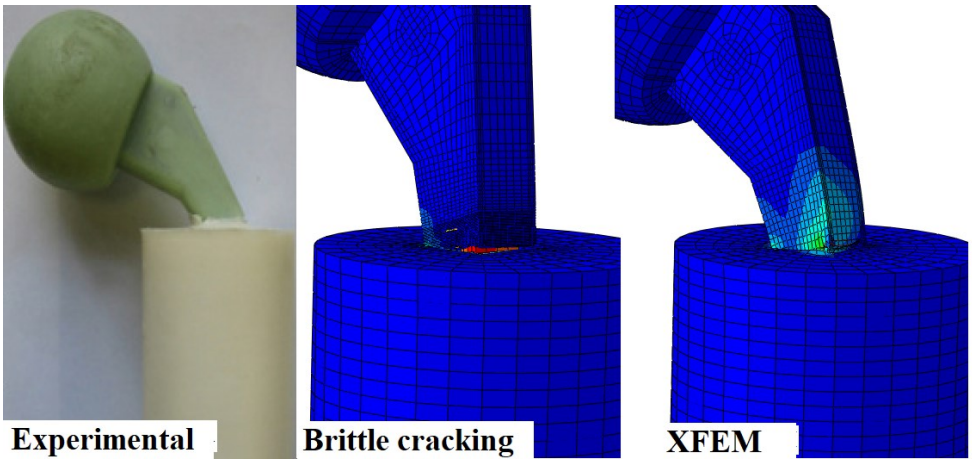

(d) Full-stem reinforced spacers with 10mm thickness endoskeleton

Fig.10 Appearance of deformed spacers at the end of the test: Experimental model [12], Brittle cracking model and XFEM model (from left to right).

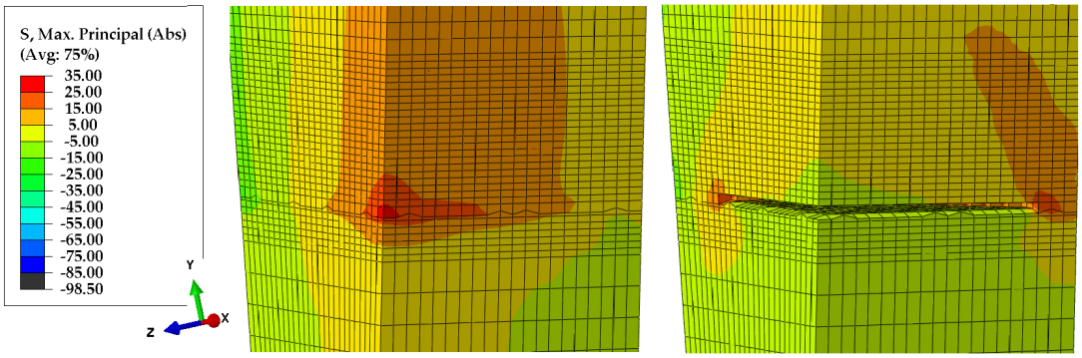

(a) Left posterior view

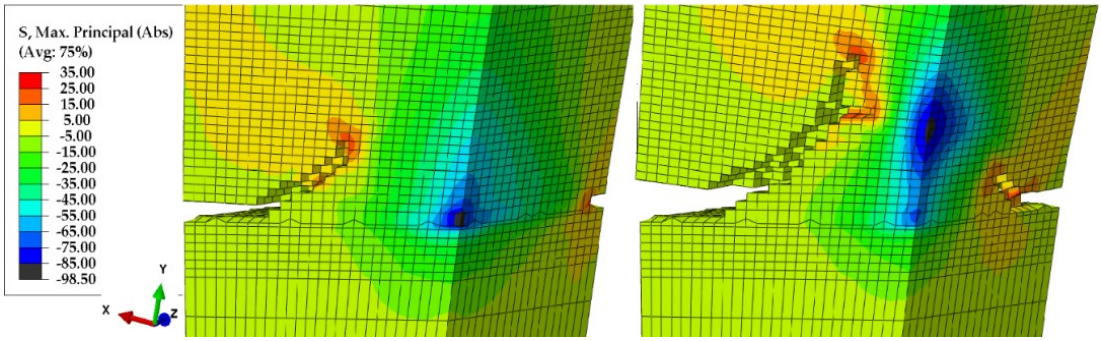

(b) Right anterior view

Fig.11 Maximum principal stress distribution in brittle cracking model

The early phases of crack propagation are illustrated by the left posterior views (Figure 11 (a)). In both models the crack initiation occurs at the left posterior facet level from the first element above the insertion of the spacer in the cylinder which is due to the inclination of the spacer (10° in the frontal plane and 9° in the sagittal plane) representing the first element recording the maximum principal stress exceeding the failure level. After crack propagation, the max stress was concentrated at crack tip taking profile as butterfly wings. The processed crack tipzone was small which indicates a behavior of brittle material failure. In the first step, the crack propagation is nearly horizontal, and the predominant loading for this phase is the mode I fracture (Fig.11(a)). In the second stage, the crack propagation is governed by a mixed-mode from which the orientation changes, where it is more visible in the brittle cracking models (Fig.11(b)).Although, the appearance of the XFEM crack model has a more natural behavior (Fig. 12); the brittle cracking trajectory, however, was similar to the experimental model. This is caused by the different stress distribution which depends on the simulated model. At the final stage, the elements contained in the ligament are subjected only to compressive stresses leading to the interruption of the crack extension.

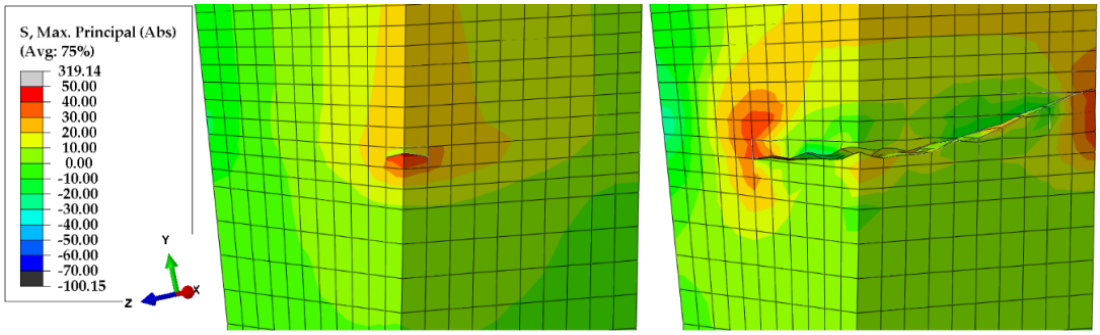

(a) Left posterior view

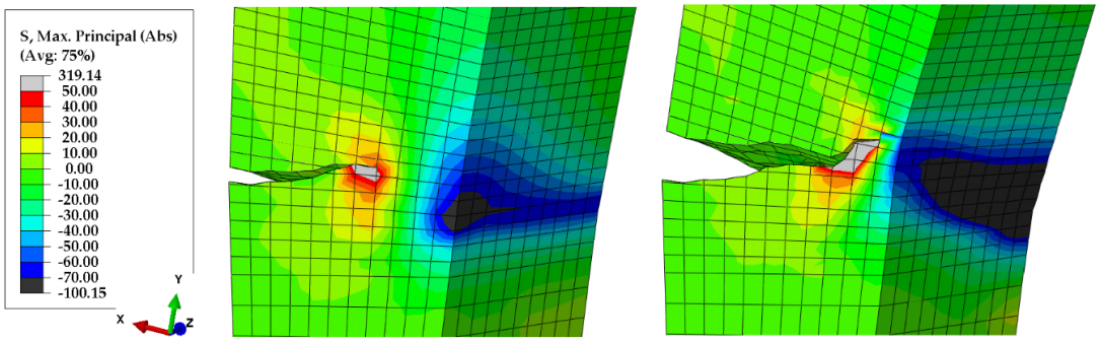

(b) Right front view

Fig.12 Maximum principal stress distribution in XFEM model

4. Optimization of spacers

Although, the fracture of spacer stem is a possible complication, it remains asymptomatic and does not require a surgical revision. However, the rupture of the neck (Fig. 15(a)) is often associated with a dislocation of the spacing head which requires the prosthesis to be replaced [9, 40]. In order to simulate the closest in vivo conditions as possible (anatomy of the upper end of the femur) a new numerical model (Fig. 13) is created in which the spacer is inserted deeper into a cylinder cut at the top and slanted. Figures 15 shows the appearance of the spacer without reinforcement of the new model at the end of the simulation. The deep insertion causes a higher level of stresses in the upper part of the spacer within the end a rupture at the level of the neck is similar to that observed in the clinic case.

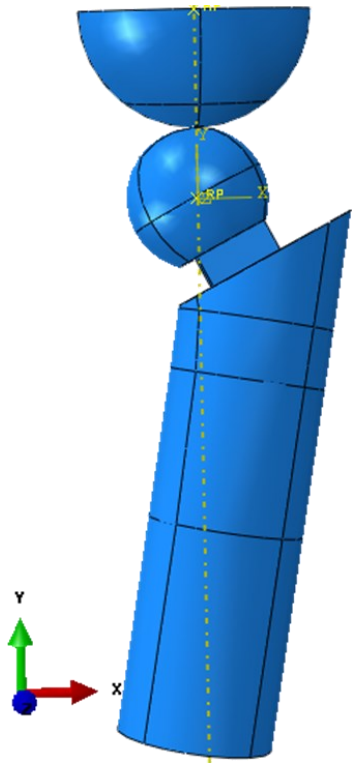

Fig. 13 New model with the spacer deeply inserted.

In order to deduce the changes of reinforcement material effect, a series of quasi-static tests were carried out by replacing the titanium stem by stainless steel and ceramic materials, respectively. The elastic properties of these two materials are summarized in Table 4. The plastic properties of annealed stainless steel were necessary [41] for the simulation of the elastoplastic behavior of the reinforced spacer, while an ultimate tensile strength of 260 MPa, and a fracture energy 25 J / m^2(Fig. 14) were used to simulate the brittle cracking of ceramic. [42-44].

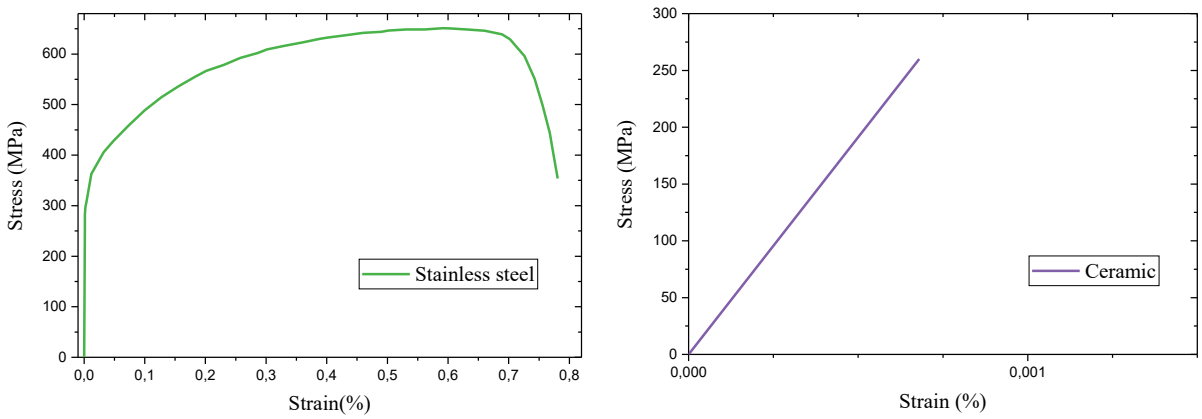

Fig. 14 Stress-strain curves of Al_2O_3 and annealed 316L stainless steel

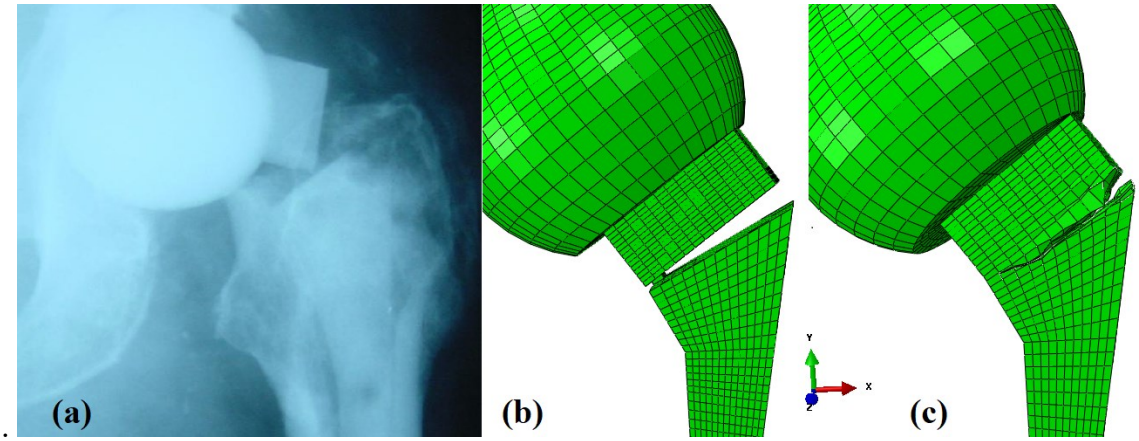

Fig. 15. Spacer's fracture at the level of the neck; from left to right: radiographic image [9], the new Brittle cracking model and the new XFEM model (from left to right).

Table 4 Elastics properties of stainless steel and ceramic [42].

Materials	Young modulus [MPa]	Poisson ratio	Density [Kg/m^3]
Stainless Steel (316L)	210000	0.35	8000
Ceramic (Al_2O_3)	380000	0.22	3900

4.1 Results and discussions

The first observation is that, the deeper insertion increases considerably the force which can support the different spacers (Fig.16). The initial slope part corresponds to the elastic behavior of the materials, which is proportional to the rigidity of the reinforcing material. The rupture behavior is dealt with differently depending on the ductile or brittle nature of the reinforcement. Due to its larger elastic limit, the spacer with Titanium reinforcement withstands greater forces than stainless steel. The spacer with a ceramic reinforcement fails

for about 40% less load. From a mechanical point of view, the use of any of the three materials can withstand the maximum transmitted force during walking [45] (representing three times the body weight) or climbing stairs [46,47] (up to six times the body weight);leading however to a permanent deformation risk by exceeding the Yield strength of 250 MPa [41,48] for the case of the 6mm reinforcement with annealed stainless steel (Fig. 17). Consequently, the purpose of the spacer is also to preserve bone longevity in expectation of the placement of the final prosthesis, to achieve this it is necessary to maintain a sufficient stress level in the femoral bone [49,50].

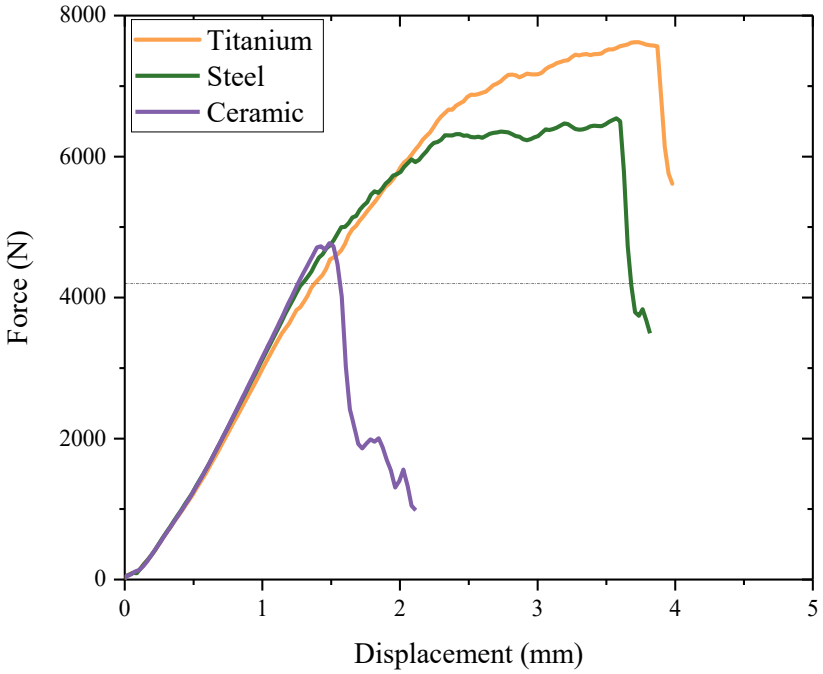

(a) Full-stem reinforced spacers with 6mm thickness endoskeleton

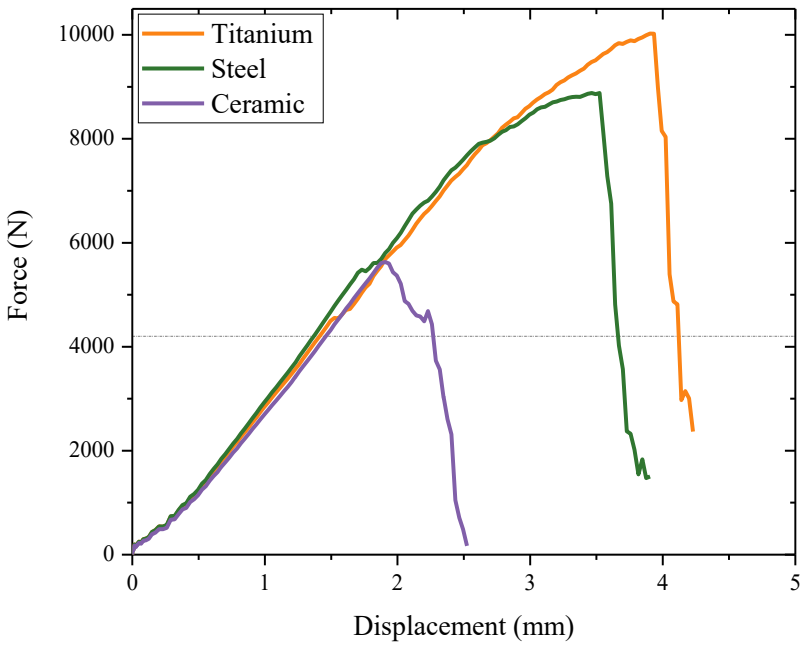

(b) Full-stem reinforced spacers with 8mm thickness endoskeleton

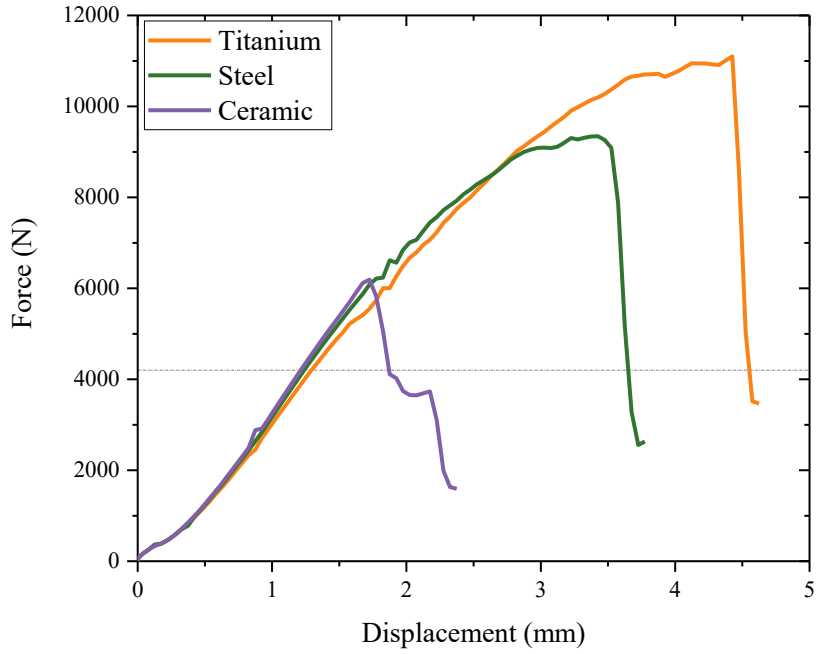

(c) Full-stem reinforced spacers with10mm thickness endoskeleton

Fig. 16: Force–displacement curves of spacers with different material's full-stem reinforcements

.

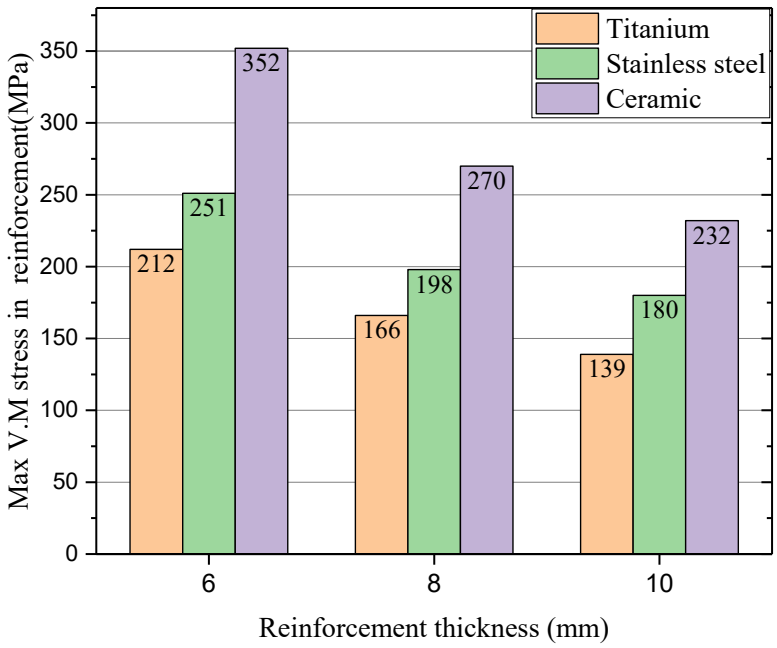

Fig. 17 Maximum von Mises stresses in the reinforcemnt for 4,2KN applied loading.

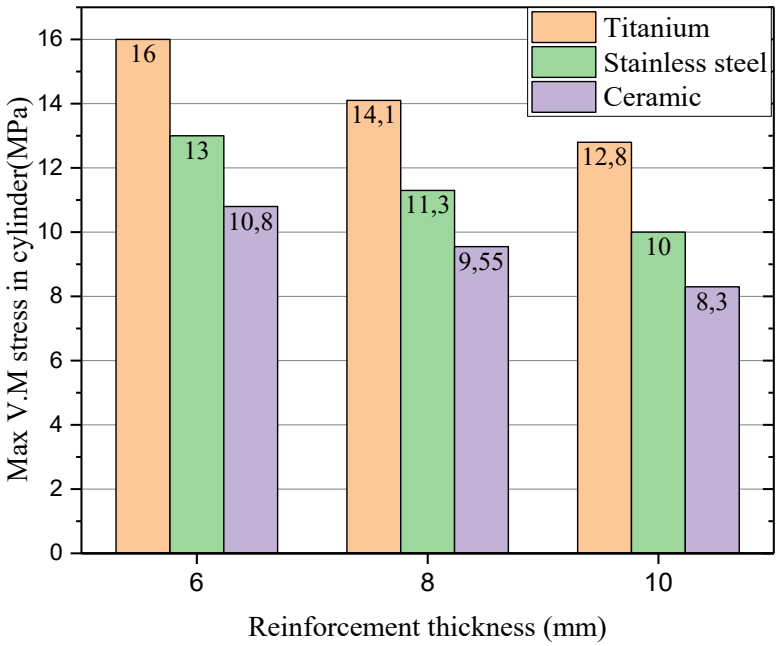

Fig. 18 Maximum von Mises stresses in the PU cylinder for 4,2KN applied loading.

In figure 18, the values of the maximum von Mises stresses calculated at the cylinder level, generated from a subjected loading of 4.2 KN on the head of the spacer (i.e. a force transmitted to the hip for a person of 70 Kg during the stair climbing) [46].The results show

that, the maximum stress at the PU cylinder decreases with the increase in the reinforcement thickness, in addition to the increase of the used material stiffness. This phenomenon is called stress shielding which can occur when some of the load is absorbed by the prosthesis instead of being transmitted to the bone [50]. Stress shielding is believed to be responsible for bone resorption [49,50]. However, other studies have demonstrated the advantages of reducing the stiffness of implants by acting on the chosen material as well as on the section of the rod in order to reduce stress shielding [52, 53].Finally from a biological point of view, the influence of the reinforcement insertion on the pharmacokinetic properties of the spacer is not certain [54], but what is certain is that the quantity of antibiotic released is proportional to cement's volume [55], showing the advantage of using the smallest possible reinforcement.

5. Conclusion

This paper proposed a validated numerical model which simulates the behavior of a hip spacer under quasi-static loading. The model was validated experimentally for four spacers types, namely non-reinforced spacer, full-stem reinforced spacers with endoskeleton of 6mm, 8mm and 10mm thicknesses respectively using load-displacement curves and crack path. The use of the explicit method associated with the brittle cracking model is a fast and efficient tool to simulate the damage of spacers subjected to a quasi-static loading, on condition of choosing an adequate loading rate and mass scaling factor. It was found that the addition of reinforcement is very important to withstand the spacer resistance due to daily activities effort. This investigation demonstrated that a 6 mm Titanium reinforcement was the optimum choice which satisfies the mechanical properties improvementof the spacer and prevents the femoral bone from failure.

References

[1] Affatato S, Mattarozzi A, Taddei P, Robotti P, Soffiati R, Sudanese A, Toni A. Investigations on the wear behaviour of the temporary PMMA-based hip Spacer-G. ProcInstMech Eng. 2003; 217(1): 1-8.

[2] Hsieh PH, Chen LH, Chen CH, Lee MS, Yang WE, Shih CH. Two-Stage Revision Hip Arthroplasty for Infection with a Custom-Made, Antibiotic-Loaded, Cement Prosthesis as an Interim Spacer. J Trauma. 2004; 56: 1247-1252.

[3] Leunig M, Chosa E, Speck M, Ganz R. A cement spacer for two-stage revision of infected implants of the hip. IntOrthop. 1998; 22: 209-214.

[4] Magnan B, Regis D, Biscaglia R, Bartolozzi P. Preformed acrylic bone cement spacer loaded with antibiotics: use of two-stage procedure in 10 patients because of infected hips after total replacement. ActaOrthop Scand. 2001; 72: 591-594.

[5] Yamamoto K, Miyagawa N, Masaoka T, Katori Y, Shishido T, Imakiire A. Cement Spacer Loaded with Antibiotics for Infected Implants of the Hip Joint. J Arthroplasty. 2009; 24(1): 83-89.

[6] Lewis G. Fatigue testing and performance of acrylic bone-cement materials: state of the art review. J Biomed Mater Res 2003;66B (1):457–86.

[7] Krause WR, Hofmann A. Antibiotic impregnated acrylic bone cements: a comparative study of the mechanical properties. J BioactCompatPolym1989; 4:345–62.

[8] R. Botchu, R. Anwar, KJ Ravikumar . FRACTURED CEMENT SPACERS—A REPORT OF TWO CASES Iowa Orthop J. 2009; 29: 17–18.

[9] K. Anagnostakos. Mechanical complications and reconstruction strategies at the site of hip spacer implantation. *International Journal of Medical Sciences* 2009; 6(5):274-279.

[10] Kummer FJ, Strauss E, Wright K, Kubiak EN, Di PE. Mechanical Evaluation of Unipolar Hip Spacer Constructs. Am J Orthop. 2008; 37(10): 517-518.

[11] Schöllner C, Fürderer S, Rompe J-D, Eckardt A. Individual bone cement spacers (IBCS) for septic hip revision – preliminary report. Arch OrthopTraumSurg. 2003; 123: 254-259.

[12] T. Thielen, S. Maas, A. Zuerbes, D. Waldmann. Development of a reinforced PMMA based hip spacer adapted to patients' needs. Medical Engineering & Physics 31 (2009) 930-936.

[13] T. Thielen, S. Maas, A. Zuerbes, D. Waldmann. Mechanical behaviour of standardized, endoskeleton-including hip spacers implanted into composite femurs. *Int. J. Med. Sci.* 2009; 6(5):280-286.

[14] Krishnamurthy N. and Graddy D. E., Correlation between 2- and 3-Dimensional Finite Element Analysis of Steel Bolted End-Plate Connections. Computers and Structures, 1976. 6: p. 381-389.

[15] Kukreti A. R., Murray T. M., and Abolmaali A., End-Plate Connection Moment-Rotation Relationship. Journal of Constructional Steel Research, 1987. 8: p. 137-157.

[16] Vegte G. J., Makino Y., and Sakimoto T., Numerical Research on Single Bolted Connections Using Implicit and Explicit Solution Techniques. Memoirs of the Faculty of Engineering, Kumamato University, 2002. 47.

[17] Bursi O. S. and Jaspart J. P., Benchmarks for Finite Element Modelling of Bolted Steel Connections. Journal of Constructional Steel Research, 1997. 43: p. 17-42.

[18] Bursi O. S. and Jaspart J. P., Calibration of a Finite Element Model for Isolated Bolted End-Plate Steel Connection. Journal of Constructional Steel Research, 1997. 44: p. 225-262.

[19] Wheeler A. T., Clarcke M. J., and Hancock G. J., FE Modelling of Four Bolt Tubular Moment End-Plate Connections. Journal of Structural Engineering, 2000. 126: p. 816-822.

[20] Abdullah R., Paton-Cole V. P., and Easterling W. S., Quasi-static analysis of composite slab. Malysian Journal of Civil Engineering, 2007. 19(2): p. 91-103.

[21] Natário P., Silvestre N., and Camotim D., Web crippling failure using quasi-static FE models. Thin-Walled Structures, 2014. 84: p. 34-49.

[22] A. Al-Rifaie, Z. W. Guan, S. W. Jones. Quasi-Static Analysis of End Plate Beam-to-Column Connections. International Scholarly and Scientific Research & Innovation 11(7) 2017.

[23] Abaqus documentations. SIMULIA.

[24] Z. Zhang, M. Thompson, C. Field, W. Li, Q. Li and M. V. Swain, Fracture behavior of inlay and onlay fixed partial dentures–an in-vitro experimental and XFEM modeling study, Journal of the Mechanical Behavior of Biomedical Materials. Volume 59, June 2016, Pages 279-290.

[25] B. Gasmi, S.Abderrahmene, B.Smail and A.Benaoumeur. Initiation and propagation of a crack in the orthopedic cement of a THR using XFEM.Advances in Computational Design, Vol. 4, No. 3 (2019) 295-305.

[26] Dippmann C. Statische und dynamische Drucktestung von PMMA Hüftinterims prothesen.PhD. Thesis. Universität des Saarlandes, Homburg/Saar; 2005.

[27] Schoellner C, Furderer S, Rompe JD, Eckhardt A (2003) Individual bone cement spacers (IBCS) for septic hip revision-preliminary report. Arch Orthop Trauma Surg 123(5):254–259

[28] N.o Kaku. T. Tabata. H. Tsumura.Mechanical evaluation of hip cement spacer reinforcement with stainless steel Kirschner wires, titanium and carbon rods, and stainless steel mesh. European Journal of Orthopaedic Surgery & Traumatology volume 25, pages489–496(2015

[29] H. Salah, M.M. Bouziane, S.M. Fekih, B. BachirBoudjra and S. Benbarek. Optimisation of a Reinforced Cement Spacer in Total Hip Arthroplasty. Journal of Biomimetics, Biomaterials and Biomedical Engineering. 2296-9845, Vol. 35, pp 35-49

[30] S. Samsami, S.Saberi, S.Sadighi&G. Rouh . Comparison of Three Fixation Methods for Femoral Neck Fracture in Young Adults: Experimental and Numerical Investigations. Journal of Medical and Biological Engineering volume 35, pages566–579(2015)

[31] M. Cilla, S. Checa, G. N. Duda. Strain shielding inspired re-design of proximal femoral stems for total hip arthroplasty. J Orthop Res 35:2534–2544, 2017

[32] Atlas of stress-strain curves 2nd edition. ASM international 2002

[33] A. Hillerborg, M. Modéer, P.E. Petersson, 1976. Analysis of crack formation and crack growth in concrete by means of fracture mechanics and finite elements. Cement Concrete Research 6 (6), 773-781.

[34] S. Mariani, U. Perego, 2003. Extended finite element method for quasi-brittle fracture. International Journal for Numerical Methods in Engineering 58 (1), 103-126.

[35] N. Moës, T. Belytschko, 2002. Extended finite element method for cohesive crack growth. Engineering Fracture Mechanics 69 (7), 813-833.

[36] G.N. Wells, L.J. Sluys, 2001. A new method for modelling cohesive cracks using finite elements. International Journal for Numerical Methods in Engineering 50 (12), 2667-2682.

[37] T. Rabczuk, G. Zi. A new crack tip element for the phantom-node method with arbitrary cohesive cracks. Int. J. Numer. Meth.Engng 2008; 75:577–599

[38] A. J. Khan et al 2016. Development of material model for assessment of brittle cracking behavior of Plexiglas. IOP Conf. Ser.: Mater. Sci. Eng. 146 012008.

[39] A. May-Pata and al.Comparative study on the mechanical and fracture properties of acrylic bone cements prepared with monomers containing amine groups. Journal of the mechanical behavior of biomedical materials .6(2012)95-105.

[40] P.Barreira, P.Leite, P. Neves. Preventing mechanical complications of hip spacer implantation. *ActaOrthop. Belg.*, 2015, 81, 344-348

[41] R. K. Blandford, D. K. Morton. Tensile Stress-Strain Results for 304L and 316L Stainless Steel Plate at Temperature.2007 ASME Pressure Vessels and Piping Division Conference. July 2007.

[42] ASM Engineered Materials Reference Book, Second Edition, Michael Bauccio, Ed. ASM International, Materials Park, OH, 1994.

[43] L. A. SIMPSON. Effect of Microstructure on Measurements of Fracture Energy of ALO, January 1973. The journal of The American Ceramic Society.

[44] Pastor, J.Y. (1993). Fractura de materiales cerámicos estructurale savanzados. PhD. Thesis. Universidad Complutense de Madrid.

[45] Bergmann, F. Graichen, A. Rohlmann: Hip joint loading during walking and running, measured in two patients. Journal of Biomechanics, 26:969–990, 1993

[46] Costigan, K. Deluzio, U. Wyss: Knee and hip kinetics during normal stair. Climbing. Gait and Posture, 16:31–37, 2002.

[47] Bergmann, G. Deuretzbacher, M. Heller, F. Graichen, A. Rohlmann, J. Strauss, G. Duda: Hip contact forces and gait patterns from routine activities. Journal of Biomechanics, 34:859–871, 2001

[48] *E. Hamidi, A. Fazel i, M. A. Mat Yajid*. Materials Selection for Hip Prosthesis by the Method of Weighted Properties. Journal of Advanced Research in Materials Science ISSN (online): 2289-7992 | Vol. 4, No.1. Pages 1-13, 2015.

[49] Bugbee WD, Sychterz CJ, Engh CA. Bone remodeling around cementless hip implants. South Med J. 1996 Nov;89(11):1036-40.

[50] T. Niinimäki, J. Junila, P. Jalovaara. A proximal fixed anatomic femoral stem reduces stress shielding. International Orthopaedics (SICOT) (2001) 25:85–88

[51] Paul J.P., Strength requirements for internal and external prostheses.J. Biomechanics,1999,32:381-393

[52] Bitsakos C, Kerner J, Fisher I, Amis AA. The effect of muscle loading on the simulation of bone remodelling in the proximal femur. J Biomech. 2005 Jan;38(1):133-9.

[53] Diegel PD, Daniels AU, Dunn HK. Initial effect of collarless stem stiffness on femoral bone strain. J Arthroplasty. 1989;4(2):173-8.

[54] Anagnostakos K, Kelm J, Grün S, Schmitt E, Jung W, Swoboda S: Antimicrobial properties and elution kinetics of linezolid-loaded hip spacers *in vitro*. Journal of Biomedical Materials Research Part B: Applied Biomaterials. 2008, 87B (1): 173-178.

[55] Richard E. Duey, MD; Alexander CM. Chong; Mechanical Properties and Elution Characteristics of Polymethylmethacrylate Bone Cement Impregnated with Antibiotics for Various Surface Area and Volume Constructs;